Nanoscale

Accepted Manuscript

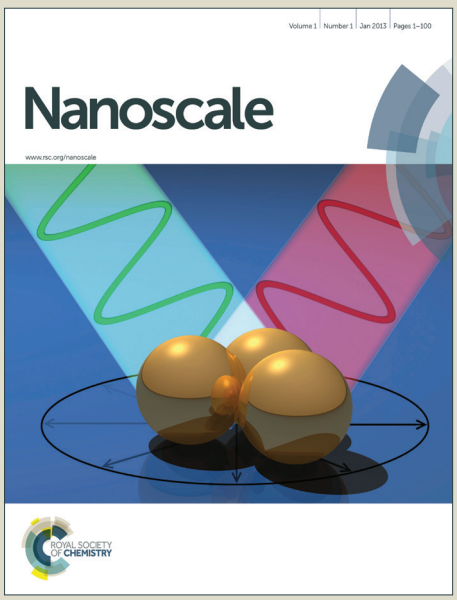

ROYAL SOCIETY OF CHEMISTRY

www.rsc.org/nanoscale

Cite this: DOI: 10.1039/c0xx00000x

www.rsc.org/xxxxxx

ARTICLE TYPE

Exploitable length correlations in peptide nanofibres

Emiliana De Santis,[a] Nilofar Faruqui,[a] James E. Noble,[a] and Maxim G. Ryadnov[ab]*

Received (in XXX, XXX) Xth XXXXXXXXX 20XX, Accepted Xth XXXXXXXXX 20XX
DOI: 10.1039/b000000x

Sequence-prescribed biomolecular assemblies find increasing use in the development of novel nanostructured materials. Critical requirements for emerging designs remain in matching form with function. Peptide assembly diversifies form and supports function, but lacks control over both. Herein we exploit length correlations in peptide nanoscale fibres (form) using a model helical template. We establish that different assembly patterns result from a synergistic interplay between peptide length, net charge and folding and supramolecular cooperativity, while correlating with increases in cell proliferation (function) as a function of peptide length. The revealed correlations offer an efficient rationale for the programming of longitudinally finite and biologically active nanoscale fibres.

Introduction

An ability to predict and control nanoscale assembly can impact on both pure and applied chemistry. Biological systems employ protein folding elements as building units that spontaneously assemble into complex architectures with specific functions. α-Helical coiled-coils, which account for 3-5% of all encoded proteins,[1] including transcription factors,[2] intermediate filaments[3, 4] and viral coats[5, 6] are ubiquitous for biomolecular self-oligomerisation and increasingly so for prescriptive bionanodesigns.

The hallmark of most coiled-coil sequences is a heptad repeat of hydrophobic ***H*** and polar ***P*** residues, ***HPPHPPP***, which is often denoted ***abcdefg***.[7] The spacing between hydrophobic residues, which are placed in ***a*** and ***d*** positions, is approximately 3.5 residues. This arrangement creates a hydrophobic seam along one side of the coiled-coil helix, which adopts a left-handed twist to accommodate 3.5 residues per turn – the spacing which is short of the repeat for monomeric right-handed α-helices (3.6-residue). Thus, two or more seams, two or more helices, can interdigitate to polymerise into longitudinal rope-like and, through lateral associations, fibrous coiled-coil structures. The architecture, oligomerisation state and morphology of resulting coiled-coil assemblies are largely defined by the very nature of amino acids used, and in particular in the hydrophobic ***a*** and ***d*** positions and electrostatic interfacial ***e*** and ***g*** sites. Such sequence-to-structure relationships combined with the synthetic accessibility of coiled coils have led to notable successes in the design of fibrous materials in recent years.[7-9] Indeed, it was shown that empirical control can be achieved over fibre thickening,[10] fibre topology,[11-13] and morphological switching from cage-like to fibrous nanostructures.[14, 15] Programmed in sequences these features can also be introduced using an alternative approach involving the use of one-heptad modules, simple re-arrangements of which in the same sequence template were shown to lead to different supramolecular fibre architectures.[16]

Despite all the progress made in engineering fibre morphology fibre designs of finite or arrested lengths are lacking. Most native coiled coils and coiled-coil filaments assemble from proteins. Having essentially no length restrictions protein sequences tend to assemble in register and into finite structures. Synthetic fibres assemble from much shorter sequences typically not exceeding 35 residues.[17] Such an imposed physical restraint stimulates the development of auxiliary strategies that can enable the axial coiled-coil propagation of short peptides. A notable approach is the use of staggered coiled-coil oligomers that polymerise longitudinally through terminal complementary overhangs.[9, 15, 18] Resulting structures are microns-long fibres with broad length distributions. In this regard, an empirical correlation between peptide and fibre lengths, which has yet to be reported, is of considerable interest. Herein, we introduce a straightforward approach exploring such correlation.

Results and discussion

Specifically, we designed a symmetrical sequence template comprising two generic α-helical modules, N- and C-terminal, with the number of heptads in both modules being exactly the same. The main variable in the template is the total number of heptads in each module. Given the minimum requirement of two contiguous heptads to promote cooperative and stable fibre formation,[16] a starting template was made of four heptads. Modules with three and four heptads provided two length variations of the template (Table 1). To promote a staggered coiled-coil assembly[17] the modules were made oppositely charged using a cationic heptad, KIAALKQ, for the N-terminal module, and an anionic heptad, EIAALEQ, for the C-terminal module, respectively (Fig. 1).

For the ***a-d*** pairs the isoleucine-leucine combination, which favours coiled-coil dimers, was used. Complementary charges at ***g*** and ***e*** sites of successive heptads (***g-e′*** interactions) were introduced to set up an axial stagger of the terminal modules.

Table 1 Sequence template with varied integral module numbers

Name[a]	Sequence			
	gabcdef	gabcde**f**	gabcdef	gabcdef
T2	(KIAALKQ)	(KIAALK**K**)	(EIAALEY)	(EIAALEQ)
T3	$(KIAALKQ)_2$	(KIAALK**K**)	(EIAALEY)	$(EIAALEQ)_2$
T4	$(KIAALKQ)_3$	(KIAALK**K**)	(EIAALEY)	$(EIAALEQ)_3$
T3(-)	$(KIAALKQ)_2$	(KIAALK**E**)	(EIAALEY)	$(EIAALEQ)_2$

[a]peptide names correspond to the template with an integral module number; a charged residue in a single ***f*** site providing an overall net charge is in bold.

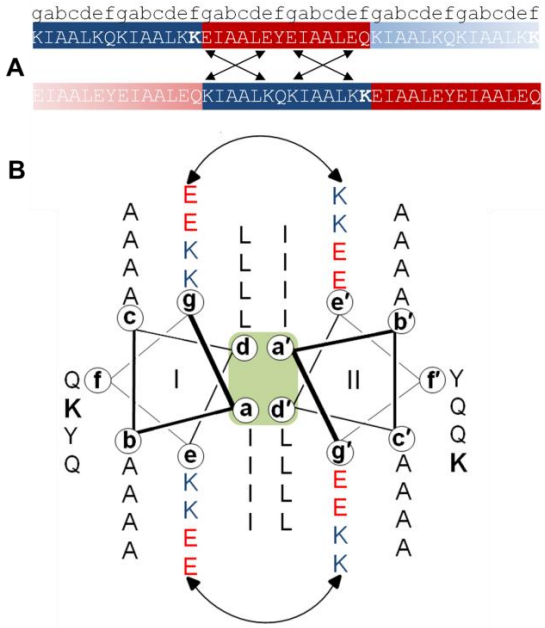

Fig. 1. Template design. (A) Cationic and anionic modules arranged into a staggered coiled-coil homodimer. (B) Coiled-coil helical-wheels of the dimer with arrows indicating stabilising electrostatic interactions and the green box signifying the hydrophobic interface. A lysine residue in a single ***f*** site providing a net positive charge is highlighted in bold. Cationic and anionic modules and residues are highlighted in blue and red, respectively.

The solvent-exposed ***b***, ***c***, and ***f*** sites were occupied by alanines and glutamines, to minimize the lateral association of coiled-coil oligomers, while a tyrosine was included in a single ***f*** site as a chromophore for accurate concentration determination (Fig. 1).[7, 16] All amino acids used are characterised by high α-helix propensity.[19] Finally, the ***f*** site of the central heptad in each sequence was made lysine to make an overall positive net charge.[17]

Consistent with the design, for all the peptides at micromolar concentrations in 10 mM MOPS, circular dichroism (CD) spectroscopy showed high degrees of α-helix.[20] As expected for helical assemblies, spectral $\Delta\varepsilon_{222}/\Delta\varepsilon_{208}$ ratios were ≥ 1 (Fig. 2A and Table S1 in Supporting Information).[21, 22] A greater conformational order for shorter peptides was ascertained by increases in helical content as a function of peptide length, with stronger helical signals recorded for shorter peptides showing ~5% drops in helicity a step in the T2>T3>T4 order (Fig. 2A, Table S1).[21, 23] Similar effects were reported by others for discrete coiled coils with nearly 10% decreases in helicity per extra heptad.[24] Furthermore, CD spectra for self-assembled systems combine contributions from α-helices in coiled coils and in the assembly, which are cumulative and may be associated with increases in helical content.[25] Therefore, the strongest helix detected for the shortest T2 may be indicative of a more stable and cooperative coiled-coil assembly when compared to the longer peptides.

Further support for this came from CD spectra recorded in 50% 2,2,2-trifluoroethanol (TFE). Fluorinated alcohols promote intramolecular hydrogen bonding by excluding water from the solute, i.e. encompassing it in a hydrophobic "matrix", and by lowering the dielectric constant.[26] The secondary structure observed in the presence of TFE would thus correspond to that of an individual peptide.[25, 27] CD spectra in 50% TFE revealed α-helical conformations for all the peptides with $\Delta\varepsilon_{222}/\Delta\varepsilon_{208}$ ratios of <1 suggesting that monomeric conformers were predominant (Fig. S1A). As expected, the percentage of α-helix increased from shorter T2 to longer T3 and T4 peptides (Fig. 2A inset). The latter two were essentially fully folded at these conditions and their CD spectra overlaid (Fig. S1A). These observations suggest a helicity cut-off at T2 beyond which the ~10% deficit for an extra heptad observed in MOPS is regained at the expense of disrupted coiled-coil interactions in the presence of 50% TFE. In good agreement with other systems[24] and with the reverse order in helix increases observed in aqueous buffers (Fig. 2A), the results suggest a higher supramolecular order for T2 (Fig. 2A and S1A).

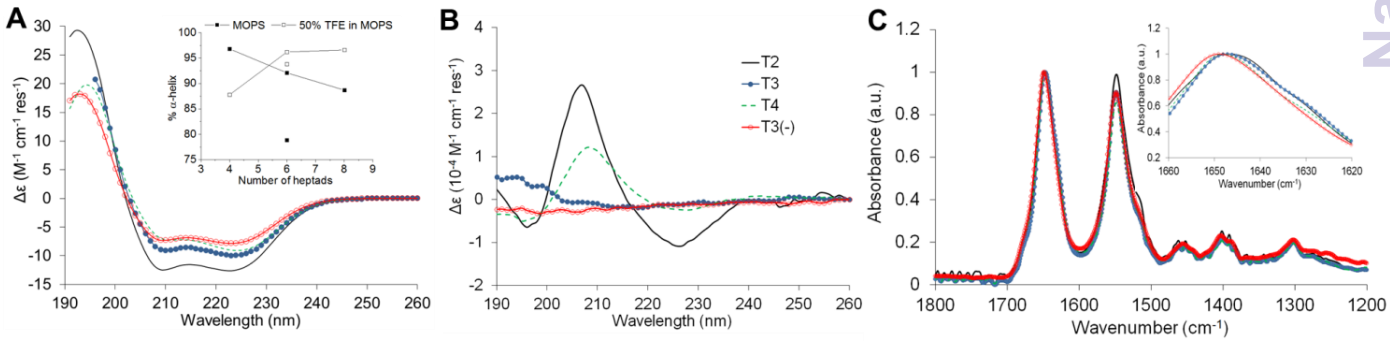

Fig. 2 Template folding. (A) CD, (B) LD and (C) FT-IR spectra for T2 (solid line), T3 (closed circles line), T4 (dashed line) and T3(-) (open circles) in 10 mM MOPS buffer at pH 7.4. Inset in A shows % α-helix as a function of peptide length (number of heptads) in MOPS and 50% TFE, closed and open squares, respectively. The points outside the lines correspond to T3(-). Inset in C shows an expanded region of the amide I band.

Indeed, as judged by transmission electron microscopy (TEM), T2 fibres were longer than T3 or T4 with average lengths of 200 ± 30 nm versus 80 ± 20 nm, and tended to entangle with the formation of branching bundles (500 ± 100 nm), which was in contrast to morphologically discrete T3 and T4 assemblies (Fig. 3). As a consequence, the latter two appeared as dense "carpets" spanning nano-to-microscale dimensions. This effect was particularly apparent for T3 fibres, which, unlike T2 and T4, showed no signs of side-by-side associations and were randomly oriented. Consistent with the TEM analysis, linear dichroism (LD) spectra, which are used as a measure of relative peptide and fibre orientation,[28] showed positive and negative bands respectively at 208 and 222 nm for T2 and T4, but not for T3 (Fig. 2B). These bands are characteristic of a peptide orientation which is parallel to the main fibre axis and is defined by fibre alignment under laminar flow.[9, 28]

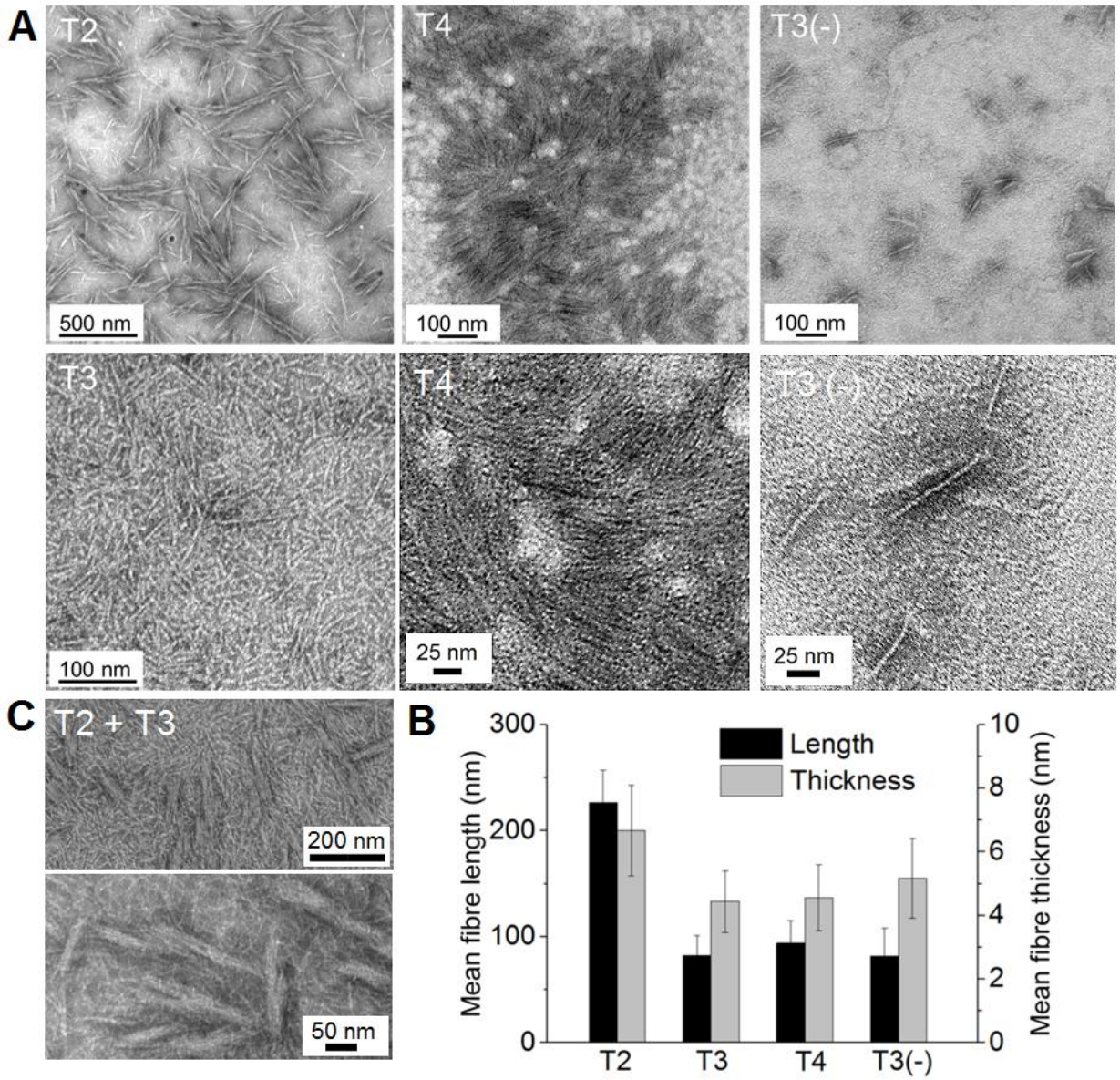

Fig. 3 Template assembly. (A) Electron micrographs of assembled templates. (B) Average fibre lengths and thicknesses shown as a function of peptide length (C) Electron micrographs of pre-assembled T2 and T3 templates mixed in 1:1 molar ratio.

No spectral features were observed for T3 thus indicating a random or poor fibre alignment, which is likely to be due to the lack of inter-fibre associations. Indeed, T3 and T4 fibres were of comparable lengths, while all three templates were characterised by the same mean diameter of 4-8 nm. Further, native gel electrophoresis experiments revealed that T3 assemblies were nearly two times smaller than T2 and T4 fibres suggesting discrete, non-associative fibre formations for T3 (Fig. S2). Fibres of both types, discrete and bundled, appeared stabilised and morphologically conserved, which was particularly evident for equimolar mixtures of pre-assembled T2 and T3, in which discrete T3 fibres were clearly contrasted with T2 bundles (Fig. 3C). These results prompt a cooperative mechanism by which 2-nm-wide coiled coils bundle up into individual fibres (3-5 coiled

coils per fibre) with different degrees of inter-fibre association. This is intriguing and might be explained from the net charge perspective. Fibres of all three templates are strongly cationic. Because (i) all three peptide templates have the same net charge (+1) and (ii) assembled fibres are of the same diameters (4-8 nm), fibre net charges will vary as a function of peptide and fibre lengths. Longer fibres assembled from shorter peptides will have more peptide molecules incorporated and hence a more extensive surface charge. Based on this rationale, the net charge of individual fibres decreases in the T2>T3>T4 order or, according to an average number of peptide molecules, in 400>67>50 (i.e. an 80x5-nm T4 fibre incorporates 10x5=50 peptides).

Although pronounced in the formed structures, this trend is not expected to lead to significant differences in the total charge densities of T fibres, which are deemed similar at the same chain concentrations used. Gratifyingly, light scattering measurements returned ζ-potential values that were comparable for all three template assemblies while being in good agreement with the observed patterns of electrophoretic mobility (Table S1 and Fig. S2). The values were characteristic of incipient stabilities, which is fully consistent with self-assembling systems that are typically remain in equilibrium,[10] and support inter-fibre associations subject to supramolecular (steric) stabilisation and conformational stability of the templates. Granted that polycations or indeed polycationic surfaces are prone to support fibrillation and aggregation, more extensive cationic surfaces can be expected to associate more.[10, 29, 30]

However, while T4 fibres appeared to co-associate, T3 did not. This may imply a cut-off for inter-fibre associations at T3 as a result of decreasing stability (lesser helix content for T4) and cooperativity in assembly (partial unfolding). Fourier transform infrared (FT-IR) and thermal unfolding experiments provided an additional insight into this. Specifically, FTIR spectra, which showed band patterns characteristic of helical conformations (amide I and II bands at 1647 and 1548 cm^{-1}) for all three templates (Fig. 2C, S1B and Table S2), revealed that the amide I bands were red-shifted when compared to a typical monomeric α-helix in water (1656 ± 2 cm^{-1}).[30] Together with an accompanying band at 1630 cm^{-1}, common for reported coiled-coil proteins,[31] the red shift can be attributed to helical adjustments or distortions in the coiled-coil superhelix.[31] These findings are supported by sigmoidal unfolding curves of T2, the first derivatives of which gave dominating transition midpoints at ≤30°C, as expected for cooperatively folded structures (Fig. S3). By contrast, multiple transition points were apparent for T3 at 35°C, 60°C and 80°C suggesting two more conformer populations. This effect was even more pronounced for T4 which gave almost linear unfolding curves, with their first derivatives characterised by multiple overlapping transitions, and were consistent with the formation of non-specific complexes (Fig S3).[32, 33]

The decreasing cooperativity in folding from T2 to T4 is important in two regards. Firstly, it appears to relate the cut-off in helicity, at T2 (Fig. 2A), with that in inter-fibre associations, at T3 (Fig. 3). Secondly, it suggests that the stability of the template assembly is strongly mediated by the net charge. To probe these two points, an anionic counterpart of T3, in which the ***f*** site of the central heptad was made glutamate, T3(-), was produced. All spectral characteristics of T3(-) were supportive of the rationale. Specifically, the template had the lowest α-helical content in buffer (Fig. 2A), marginally weaker helix in 50% TFE (Fig. S1A) and similar (negative) ζ-potential values (Table S1) when compared to its cationic counterpart. The amide I band for T3(-) was less red-shifted being closer to that for a monomeric α-helix (1649 cm^{-1}) while completely lacking the 1630 cm^{-1} band, which was particularly evident from the second derivative spectra (Fig. 2C and S1B). LD spectra showing no specific orientation were nearly identical to those for T3, (Fig. 2B) which should be expected provided that T3(-) did not form longer fibres than T3 and did not associate into bundled structures as T2 and T4 did. Indeed, as gauged by TEM, it was observed (Fig. 3A). Further, the lower stability of the T3(-) assembly, which led to lower fibre densities, was in perfect agreement with lower size distributions by native gel electrophoresis (Fig. S2). The folding of the template however was comparably cooperative with that of T2, with a similar transition midpoint at ≥30°C (Fig. S3). Thus, it can be concluded that T3(-) tends to form stable lower oligomers with a compromised ability, by the negative net charge, for supramolecular polymerisation when compared to the other templates.

With peptide fibres bearing structural and functional similarities with the native extracellular matrices (ECM)[34] we tested the assembled templates as cell-supporting scaffolds using human dermal fibroblasts. The cells were seeded on all four template substrates and control substrates including bare plastic, taken as a background, and a collagen type I substrate used as a positive ECM control.

PrestoBlue® cell proliferation and viability assays, which provide quantitative enzymatic redox indicators of metabolically active cells, revealed that template-coated substrates strongly promoted cell adhesion and proliferation, with cells remaining viable over several days (Fig. 4 and S4). The results were also confirmed by complementary CyQUANT® cell assays, which do not depend on the metabolic activity of cells, but provide a direct measure of total cell numbers based on the total nucleic acid content (Fig. 4B and S4).

Obtained values, expressed as a percentage of total cells, CyQUANT®, and total viable cells, PrestoBlue®, showed similar trends (days 1 and 4), with cell proliferation increasing with the increased peptide length. Correlations with fibre length that are linearly related to cooperativity in folding, which decreased from T2 to T4, were expectedly reverse. Notably, short, but dense, T4 fibres promoted cell proliferation with an efficiency nearing 90% of that of fibrous collagen, whereas the longest, but individually more discrete, T2 fibres gave the lowest proliferation rates (Fig. 4B and S4). Strikingly different was the cell behaviour on the T substrates. While on condensed and oriented "carpets" of T4 fibres even proliferation patterns were apparent, cells on the other substrates tended to align and stretch around circular voids (Fig. 4 and S4).

The exact nature of this phenomenon remains unclear. However, with the comparable charge densities (Table S1), it presumably involves cell-fibre co-adjustments suggesting an instructive, and possibly inhibitory, mechanism of cell proliferation flow depending on fibre morphology. For T3 the effect was more evident at high-density cell seeding which was accompanied by notable cell stretching along the void edges (Fig. S4). Equal

explanations for this could be that cells drive away or orient the amorphous T3 "carpets", regardless of the available fibre density and charge as similar effects were observed for T3 and T3(-).

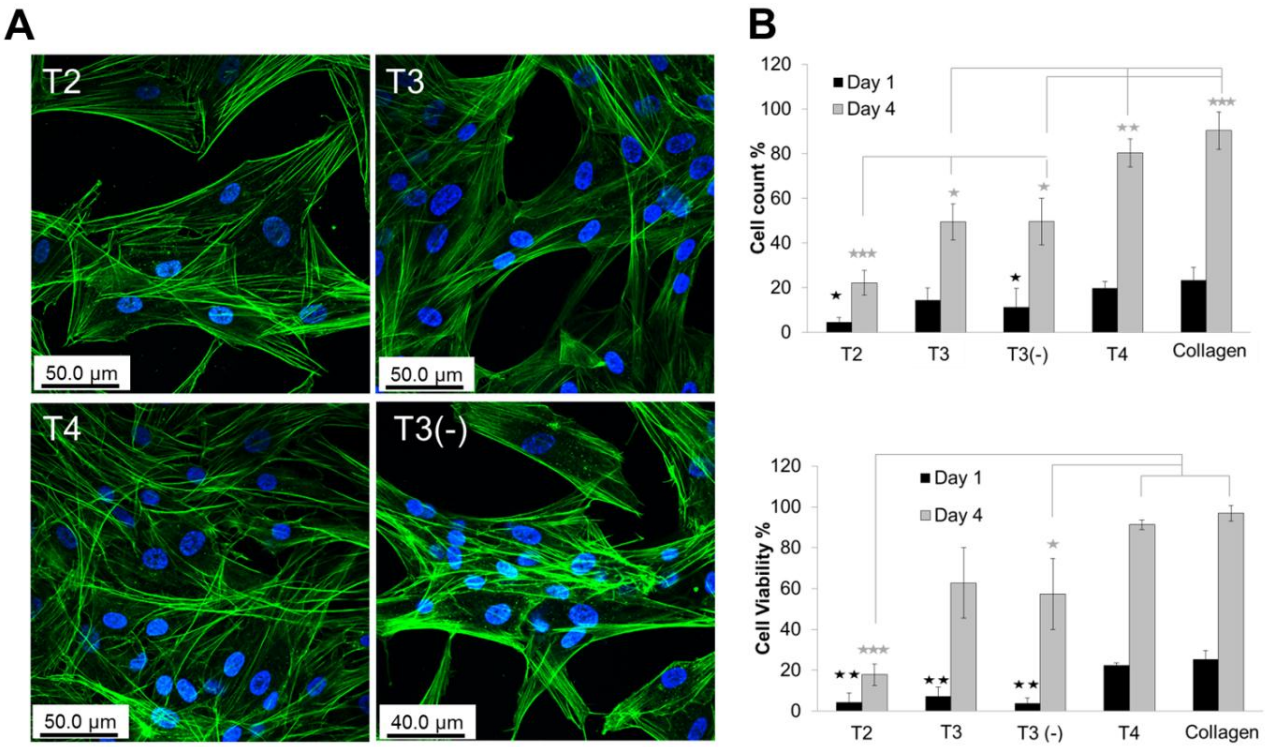

Fig. 4 Cell adhesion and proliferation . (A) Fluorescence micrographs of human dermal fibroblasts incubated for one day on template-coated substrates. Fluorescent stains Alexa-Fluor 488 phalloidin and 4′,6-diamidino-2-phenylindole highlight actin (green) and nuclear DNA (blue), respectively. (B) Cell counts, total (upper) and total viable (lower) determined by CyQUANT® and PrestoBlue® assays, respectively. Total number of cells on collagen type I on day 4 was taken as 100% after subtracting the background adhesion (bare plastic). Statistical data: (upper) cell numbers on T2 and T3(-) substrates were significantly reduced ($p<0.05$) when compared to those on T4 and collagen substrates on day 1. T2, T3 and T3(-) substrates had significantly reduced cell numbers ($p<0.001$) in comparison to collagen and T4 substrates, while T3 and T3(-) substrates had significantly reduced cell numbers ($p<0.01$) in comparison to T4 substrates, and cell numbers on T2 were significantly reduced ($p<0.05$) when compared to T3 and T3(-). (Lower) cells grown on T2, T3 and T3(-) substrates had significantly reduced viability on day 1 ($p< 0.01$) in comparison to T4 and collagen. T2 had significantly reduced viability on day 4 ($p<0.001$) in comparison to T4 and collagen substrates. T3 had significantly reduced viability ($p<0.05$) when compared to T4 and collagen substrates.

Conclusions

Using a helical model we have demonstrated exploitable correlations in supramolecular peptide fibres. Empirical inter-relationships were established between peptide and fibre lengths as a synergistic interplay of net charge and supra-molecular cooperativity. The interplay was found (i) to support extensive inter-molecular interactions – otherwise impossible within a peptide sequence space, which is substantially shorter, and (ii) to reversely correlate with peptide length, with the shortest sequence assembling into longer fibres. The synergy in interactions led to a conserved fibre thickness, observed for all templates, and enabled different co-association patterns of assembled nanofibres suggesting biologically relevant correlations. Probed in cell culture the revealed differences correlated with cell proliferation rates that increased as a function of peptide length, and with proliferation patterns specified by fibre associations.

All in all, the established correlations offer an efficient and, to the best of our knowledge, the first rationale for the programming of finite and biologically functional supramolecular fibres, the impact of which can be enhanced by combinatorial investigations using fibre systems based on other folding motifs that may provide a greater insight into exploitable sequence-fibre relationships.

Acknowledgements

We thank the NMS strategic research programme for funding, and Bill Cowley and David Everest from Animal Health and Veterinary Laboratories Agency (AHVLA) for their help with TEM.

Notes and references

[a]*National Physical Laboratory, Hampton Road, Teddington, Middlesex, TW11 0LW, UK.* [b]*School of Physics and Astronomy , University of Edimburgh, Edimburgh, EH9 3JZ, UK . Tel: 020 89436078; E-mail: max.ryadnov@npl.co.uk*

† Electronic Supplementary Information (ESI) available: materials and methods together with additional tables and figures.

1. O. J. L. Rackham, M. Madera, C. T. Armstrong, T. L. Vincent, D. N. Woolfson and J. Gough, *J Mol Biol*, 2010, **403**, 480-493.
2. E. K. O'Shea, J. D. Klemm, P. S. Kim and T. Alber, *Science*, 1991, **254**, 539-544.
3. S. Takeda, A. Yamashita, K. Maeda and Y. Maeda, *Nature*, 2003, **424**, 35-41.
4. S. V. Strelkov, H. Herrmann, N. Geisler, T. Wedig, R. Zimbelmann, U. Aebi and P. Burkhard, *EMBO J*, 2002, **21**, 1255-1266.
5. D. C. Chan, D. Fass, J. M. Berger and P. S. Kim, *Cell*, 1997, **89**, 263-273.

6. Y. Q. Deng, J. Liu, I. Zheng, W. Yong and M. Lu, *Structure*, 2006, **14**, 889-899.
7. D. N. Woolfson, *Fibrous Proteins: Coiled-Coils, Collagen and Elastomers*, 2005, **70**, 79-112.
8. S. Kojima, Y. Kuriki, T. Yoshida, K. Yazaki and K. Miura, *Proc. Japan Acad. Series B-Phys. Biol. Sci.*, 1997, **73**, 7-11.
9. M. J. Pandya, G. M. Spooner, M. Sunde, J. R. Thorpe, A. Rodger and D. N. Woolfson, *Biochemistry*, 2000, **39**, 8728-8734.
10. D. Papapostolou, E. H. C. Bromley, C. Bano and D. N. Woolfson, *J Am Chem Soc*, 2008, **130**, 5124-5130.
11. A. Bella, S. Ray, M. Shaw and M. G. Ryadnov, *Angew. Chem. Inter. Ed.*, 2012, **51**, 428-431.
12. N. L. Ogihara, G. Ghirlanda, J. W. Bryson, M. Gingery, W. F. DeGrado and D. Eisenberg, *Proc. Natl. Acad. Sci. USA*, 2001, **98**, 1404-1409.
13. M. G. Ryadnov and D. N. Woolfson, *Angew. Chem. Inter. Ed.*, 2003, **42**, 3021-3023.
14. M. G. Ryadnov, *Angew. Chem. Inter. Ed.*, 2007, **46**, 969-972.
15. S. A. Potekhin, T. N. Melnik, V. Popov, N. F. Lanina, A. A. Vazina, P. Rigler, A. S. Verdini, G. Corradin and A. V. Kajava, *Chem Biol*, 2001, **8**, 1025-1032.
16. M. G. Ryadnov, A. Bella, S. Timson and D. N. Woolfson, *J Am Chem Soc*, 2009, **131**, 13240-13241.
17. D. Papapostolou, A. M. Smith, E. D. T. Atkins, S. J. Oliver, M. G. Ryadnov, L. C. Serpell and D. N. Woolfson, *Proc. Natl. Acad. Sci. USA*, 2007, **104**, 10853-10858.
18. H. Dong, S. E. Paramonov and J. D. Hartgerink, *J Am Chem Soc*, 2008, **130**, 13691-13695.
19. A. Chakrabartty, T. Kortemme and R. L. Baldwin, *Prot. Sci.*, 1994, **3**, 843-852.
20. G. Böhm, R. Muhr and R. Jaenicke, *Prot. Eng*, 1992, **5**, 191–195.
21. S. M. Kelly, T. J. Jess and N. C. Price, *Bioch. Biophys. Acta-Proteins and Proteomics*, 2005, **1751**, 119-139.
22. T. M. Cooper and R. W. Woody, *Biopolymers*, 1990, **30**, 657-676.
23. N. J. Greenfield, *Nat Protoc*, 2006, **1**, 2876-2890.
24. J. R. Litowski and R. S. Hodges, *J Pept Res*, 2001, **58**, 477-492.
25. N. E. Zhou, B. Y. Zhu, C. M. Kay and R. S. Hodges, *Biopolymers*, 1992, **32**, 419-426.
26. D. Roccatano, G. Colombo, M. Fioroni and A. E. Mark, *Proc. Natl. Acad. Sci. USA*, 2002, **99**, 12179-12184.
27. S. Y. Lau, A. K. Taneja and R. S. Hodges, *J Biol Chem*, 1984, **259**, 13253-13261.
28. B. M. Bulheller, A. Rodger, M. R. Hicks, T. R. Dafforn, L. C. Serpell, K. E. Marshall, E. H. C. Bromley, P. J. S. King, K. J. Channon, D. N. Woolfson and J. D. Hirst, *J Am Chem Soc*, 2009, **131**, 13305-13314.
29. J. Goers, V. N. Uversky and A. L. Fink, *Prot. Sci*, 2003, **12**, 702-707.
30. J. Kong and S. Yu, *Acta Bioch. Bioph. Sinica*, 2007, **39**, 549-559.
31. T. Heimburg, J. Schunemann, K. Weber and N. Geisler, *Biochemistry*, 1999, **38**, 12727-12734.
32. R. Fairman, H. G. Chao, L. Mueller, T. B. Lavoie, L. Y. Shen, J. Novotny and G. R. Matsueda, *Prot. Sci.*, 1995, **4**, 1457-1469.
33. J. Y. Su, R. S. Hodges and C. M. Kay, *Biochemistry*, 1994, **33**, 15501-15510.
34. C. M. Kielty and C. A. Shuttleworth, *Microsc. Res. Tech.*, 1997, **38**, 413-427.